

Interface-Engineered Plasmonics in Metal/Semiconductor Heterostructures

Chuancheng Jia, Xinxi Li, Na Xin, Yao Gong, Jianxin Guan, Linan Meng, Sheng Meng, and Xuefeng Guo*

Plasmonic manipulation of light in metal/semiconductor heterostructures is a powerful tool that exploits extraordinary optical properties of metallic nanostructures to concentrate and control light at the nanometer scale. Here, recent progresses in the mechanism and strategies developed for the control of plasmon-induced optical field distribution, hot electron injection and energy transfer at the metal/semiconductor heterostructure interface are discussed. This is of crucial importance to the selection of matched materials, the design of optimized device architectures and the future development of efficient fabrication technologies for plasmon-enhanced photocatalytic and photovoltaic applications.

1. Introduction

Plasmonic nanostructures have significant abilities to concentrate light energy at the nanoscale, which comes from their nature as a collective oscillation of surface electrons of the metal with incident light at matched frequencies.^[1] When metals are hybridized with semiconductors, such nanoscale light manipulation ability of plasmonics could be utilized to improve the efficiency of photoexcitation in the semiconductors. By taking advantage of this property, diverse plasmonic metal/semiconductor heterostructures have been fabricated and widely used in different fields, such as photovoltaics, photocatalysis, photodetector, and so on.^[2]

Dr. C. Jia, X. Li, N. Xin, Y. Gong, J. Guan, Prof. X. Guo
Beijing National Laboratory for Molecular Sciences
State Key Laboratory for Structural Chemistry of
Unstable and Stable Species
College of Chemistry and Molecular Engineering
Peking University
Beijing 100871, P. R. China
E-mail: guoxf@pku.edu.cn



X. Li
School of Materials and Energy
Guangdong University of Technology
Guangzhou 510006, P. R. China
L. Meng, Prof. S. Meng
Institute of Physics
Chinese Academy of Sciences
Beijing 100190, P. R. China

Prof. X. Guo
Department of Materials Science and Engineering
College of Engineering
Peking University
Beijing 100871, P. R. China

DOI: 10.1002/aenm.201600431

Among these studies, the plasmon-induced effects on light, energy and carrier at the metal/semiconductor contact interface play the decisive role in the performance of the hybrid nanostructures. Here, we aim to timely summarize recent systematic progresses on the investigations of the working mechanisms and influencing factors of plasmon-induced electromagnetic field enhancement, plasmonic hot electron generation/injection, and energy transfer effects at the metal/semiconductor interface, as well as the strategies developed for controlling and utilizing these

interfacial effects for specific applications of the metal/semiconductor nanocomposites. For other various aspects of plasmonic energy conversion, such as plasmon-induced hot electron generation at nanoparticle/metal-oxide interfaces^[2g] and the effects of plasmonic dephasing/geometry on solar energy harvesting,^[2h] interested readers are recommended to learn previous excellent reviews (Ref. [2] and references therein).

2. Plasmon-Induced Interfacial Electromagnetic Field Enhancement

Due to the plasmonic resonance properties of metal nanostructures, a powerful ability of metallic nanostructures is to concentrate light into deep-subwavelength volumes. In this section, we focus an overview on plasmon-induced light manipulation at the metal/semiconductor interface, a crucial factor for plasmonic enhancement applications of metal/semiconductor heterostructures, which was unfortunately neglected in a few previous excellent reviews^[1a,b] where only light concentration and manipulation by intrinsic nanometallic structures have been summarized.

2.1. Coupling Between Plasmonic Metals and Dielectric Semiconductors

In metal/semiconductor heterostructures, the intrinsic plasmon-induced light scattering effect of plasmonic metals can scatter light into the underlying semiconductor layer, especially for metallic nanoparticles with large sizes (>50 nm).^[3] In addition to this fact, the screening effect of dielectric semiconductors could affect the intrinsic plasmon resonance of plasmonic nanostructures, which could be used for enhancing light concentration at the metal/semiconductor interface. In detail,

the screening caused by the dielectric surface of the semiconductor can be equivalent to a potential generated by an image of the charged plasmonic nanostructure with a factor of $(\epsilon - 1)/(\epsilon + 1)$, where ϵ is the permittivity of the semiconductor. The interaction between a plasmonic nanostructure and its image in an adjacent semiconductor introduces plasmonic coupling at the interface. For instance, for an individual plasmonic nanoparticle on a dielectric substrate (Figure 1a,b), the plasmonic nanoparticle with parallel p-polarization to the substrate could be coupled with its charged image and lead to the enhanced energy localization at the interface. Such nanoparticle-substrate interactions could be further strengthened for the case of perpendicular s-polarization, which facilitates the localization of charges near the substrate surface. Another feature of the screening effect is its permittivity dependence. In general, the substrate with larger permittivity leads to a stronger particle “image” interaction and thus enhance the plasmonic coupling at the interface.^[4] For a given metal/semiconductor heterostructure, such interfacial coupling between metallic nanostructures and semiconductors could be enhanced by cladding the metal with an extra dielectric layer of high permittivity (high- k). For instance, in the hybrid system comprising Au nanoparticle and TiO₂ nanotubes, when Au nanoparticles were covered by a layer of high- k Al₂O₃ with a thickness of 2.6 nm, the concentrated light energy could be further enhanced at the Au/TiO₂ interface and penetrate more deeply into the TiO₂ layer.^[5]

For plasmonic nanostructures with high-order symmetry, the adjacent dielectric semiconductor layer could lead to symmetry breaking through substrate-induced resonant coupling with the original plasmon modes. For example, for a plasmonic nanocube as showed in Figure 1c, it has a bright mode with finite dipole moments, which can be coupled with incident light, and a dark quadrupolar mode with zero dipole moments, which could not be efficiently coupled with light. When the plasmonic nanocube is placed close to the dielectric semiconductor, substrate-induced coupling and interference between the bright dipolar cube mode and the dark quadrupolar cube mode can give rise to the Fano resonances in the heterostructures, which form hybridized bonding (D) and antibonding (Q) plasmon resonance modes at the interface (Figure 1d).^[6] With electron energy-loss spectroscopy (EELS) and scanning transmission electron microscope (STEM) measurements, Li et al.^[7] have spatially and spectrally studied the interaction between individual Ag nanocubes and dielectric substrates. Their results illustrated that the substrate-induced Fano resonances of the plasmonic nanocube can effectively concentrate light energy to the metal/semiconductor interface. Furthermore, the concentrated energy can be further transferred to the semiconductor layer by plasmon-induced resonant energy transfer (PIRET) or direct electron transfer (DET) processes, which can be used for photovoltaic and photocatalytic applications.

In addition to the dielectric screening-induced plasmonic enhancement at the metal/semiconductor interface, when a thin transparent oxide layer with low dielectric constant is sandwiched between metals and semiconductors, the sandwiched oxide layer could form a low-loss plasmonic nanocavity at the metal/semiconductor interface. Such a plasmonic nanocavity could effectively concentrate light energy to the interface for further exciting the adjacent semiconductor layer. For instance,



Xuefeng Guo received his Ph.D. in 2004 from the Institute of Chemistry, Chinese Academy of Sciences, Beijing. From 2004 to 2007, he was a postdoctoral research scientist at the Columbia University Nanocenter. He joined the faculty as a professor under “Peking 100-Talent” Program at Peking University in 2008.

His current research is focused on nanometer/molecular electronics, organic/flexible electronics and single-molecule detection.

with a 5-nm silicon dioxide (SiO₂) layer sandwiched between an atomically smooth epitaxial Ag film and a single semiconductor nanorod, which consists of an indium gallium nitride (InGaN) core as gain medium and a gallium nitride (GaN) shell, a plasmonic nanocavity could be formed at the interface between the Ag film and the semiconductor nanorod (Figure 1e). This plasmonic nanocavity dramatically shrunk the surface plasmon polariton (SPP) excitation of the Ag film into the confined space around the nanorod, thus realizing the plasmon amplification of laser emission from the GaN gain medium.^[8] In another example, when a high refractive index GaAs nanowire with a thin low refractive index oxide layer was almost totally covered by a “Ω”-shaped resonant Au layer, a plasmonic nanocavity at the oxide layer was formed around the whole GaAs nanowire (Figure 1f). The plasmonic excitation of the “Ω”-shaped Au film with spectrally and spatially tunable resonant modes could effectively concentrate light to the confined cavity around the nanowire, which increased the quantum efficiency of the GaAs nanowire with an order of magnitude.^[9]

2.2. Coupling Between Plasmonic Hot Spots and Dielectric Semiconductors

At deep subwavelength region, the plasmonic hybridization induced by near-field interaction between adjacent plasmonic nanostructures could significantly enhance the density of the local electromagnetic field at plasmonic hot spots. Such plasmonic hot spots can be further coupled with the adjacent dielectric semiconductor by the screening effect and effectively concentrate light to the metal/semiconductor interface.^[1b,10] For instance, when metallic nanoparticles spreading on the TiO₂ substrate, both theoretical and experimental studies have illustrated that the dielectric screening effect of TiO₂ substrates could shift the hot spots of interparticle coupling from the center of the nanoparticle gap to the TiO₂ surface, thus leading to the enhanced electromagnetic field at the interface.^[11] Such electromagnetic field concentration at interfacial hot spots can be further enhanced by adding an underlying reflective plane

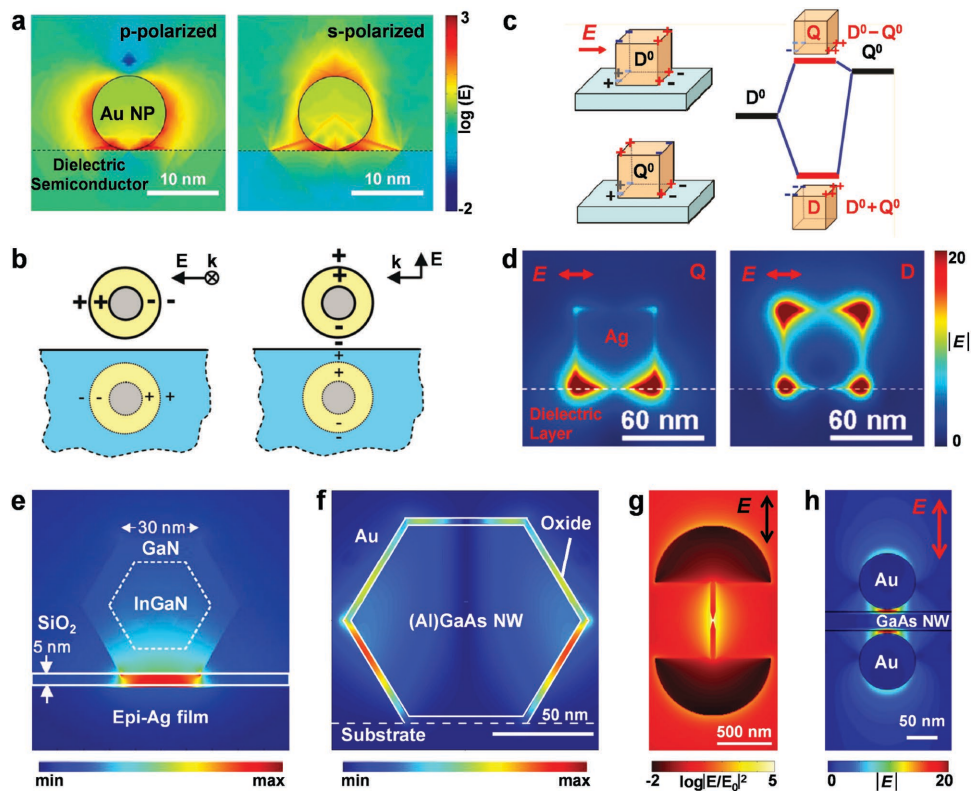


Figure 1. Plasmon-induced electromagnetic field enhancement at the metal/dielectric semiconductor interface. a,b) Electric field distribution (a) and dipolar charge distribution (b) for an individual plasmonic Au nanoparticle (Au NP) on a dielectric semiconductor under p-polarized (left) and s-polarized (right) incident lights. c) Schematic illustration of the formation of hybridized bonding D and antibonding Q modes due to substrate-mediated D_0 and Q_0 interactions. d) Electric field amplitude for a plasmonic Ag cube on a dielectric substrate at substrate-induced Fano resonance Q and D modes. e) Energy-density distribution for an individual InGaN@GaN core-shell nanorod on a SiO_2 -covered epitaxial Ag film. f) Electromagnetic density distribution across the cross-section of a (Al) GaAs nanowire core/native oxide shell/ Ω -shaped Au nanocavity. g) Electric field distribution for a plasmonic fan antenna. h) Near-field distribution of an Au nanoantenna coupled GaAs nanowire system. a) Reproduced with permission.^[20] Copyright 2013, American Chemical Society; b) Reproduced with permission.^[4] Copyright 2009, American Chemical Society; c) Reproduced with permission.^[6] Copyright 2011, American Chemical Society; d) Reproduced with permission.^[6] Copyright 2011, American Chemical Society; e) Reproduced with permission.^[8] Copyright 2012, American Association for the Advancement of Science; f) Reproduced with permission.^[9] Copyright 2014, American Chemical Society; g) Reproduced with permission.^[12] Copyright 2015, American Chemical Society; h) Reproduced with permission.^[14] Copyright 2014, American Chemical Society.

on the other side of the dielectric layer. For a fan-rod plasmonic antenna on a SiO_2 dielectric layer (Figure 1g), Brown et al.^[12] found that an added Au film under the dielectric layer could effectively increase the interfacial electromagnetic field for both fan and rod parts of the antenna by a factor of 5–6, which is ascribed to the scattered-wave interference from the underlying Au mirror. In addition to the interference effect, when the spacing between plasmonic nanocrystals and underlying metal films is close enough, the plasmonic antennas can be coupled with the metal film. This interaction affects the intrinsic plasmon resonance of the antennas and then enhances the plasmonic resonance at the interface. For instance, when an Al nanoparticle was coupled with an Al film that was separated by a ≈ 6 nm Al_2O_3 layer, the linewidth of the dipolar plasmon resonance for the Al nanoparticle could be narrowed by more than half, thus increasing the plasmonic scattering efficiency at the interface.^[13]

In addition to the heterostructures with plasmonic nanoantennas on one side of the semiconductor layer, the

semiconductor nanomaterials can be sandwiched in the gap of plasmonic nanoantennas, which could realize more effective couplings between the plasmonic mode of nanoantennas and the photonic mode of semiconductor nanomaterials. For instance, Casadei et al.^[14] have studied the plasmonic-photonic coupling between dimer metal nanoantennas and single semiconductor nanowires (NWs). Specifically, for individual GaAs NWs with ≈ 70 nm diameter sandwiched in the 90 nm gap of Au dimer nanodisks, both longitudinal and transverse plasmonic polarizations of Au dimer antennas could be effectively coupled with the NWs. Herein, for the transverse polarization, the coupling between the plasmonic antennas and the NWs is strong, and the localized electromagnetic field in the feed-gap regions of nanoantennas not only could be confined to the outside surface of the NWs, but also penetrate into the NWs (Figure 1h). Therefore, such resonant coupling between plasmonic dimer antennas and semiconducting NWs can efficiently concentrate light to semiconductor nanomaterials for further applications.

2.3. Applications of Plasmon-Induced Light Concentration

The coupling between plasmonic antennas and dielectric semiconductors or its further interaction with the interparticle-coupled hot spots of plasmonic antennas can effectively concentrate light to the metal/semiconductor interface for a variety of plasmonic enhancement applications, such as photovoltaic conversion, photocatalytic reaction, photodetector, photoluminescence and quantum information manipulation.^[15] For photovoltaic applications, by studying a model system with an atomically flat dielectric TiO₂/dye/graphene/plasmonic metal interface (Figure 2a), we have confirmed that the substrate-induced plasmons could concentrate light to the dye layer for improving the photoexcitation process, thus enhancing the photoelectric conversion efficiency.^[11] With an octahedral Ag nanocrystal decorated on a single-nanowire silicon solar cell, Brittman et al.^[16] found that the interaction between the plasmon resonance mode of Ag nanocrystals and the photonic mode of silicon nanowires could concentrate light into the nanowire for increasing the photocurrent of the solar cell. For photocatalytic reactions, especially the water splitting reaction, such

plasmonic enhancement effect at the metal/semiconductor interface was widely used for increasing the photocatalytic efficiency. For instance, several hybrid plasmonic metal/hematite (Fe₂O₃) nanostructures, such as Au nanoparticles scattered on the surface of Fe₂O₃ films,^[17] Fe₂O₃ nanorod arrays incorporated into an Au nanohole array pattern,^[18] and Si–Al–Fe₂O₃ core–multishell nanowires,^[19] have been fabricated for utilizing the plasmonic enhancement effect at the heterointerfaces to concentrate light into Fe₂O₃, which was used for enhancing the photocatalytic oxygen-producing process at Fe₂O₃ photoanodes. In addition, the electromagnetic field concentrated at the heterointerfaces can be coupled with plasmon-induced hot electrons for generating and separating more hot carriers for photocatalytic reactions. For example, hybrid nanomaterials with Au nanoparticles directly decorated on TiO₂ nanowires^[20] or with Au nanodisk antennas/thin TiO₂ films/underlying Au mirror structures (Figure 2b)^[21] have been prepared for effectively utilizing interface-enhanced hot carriers for photoelectrochemical water splitting. In photodetecting devices, Zheng et al.^[22] integrated Al grating into a metal–semiconductor–metal photodetector by using a Al grating/50 nm SiO₂/Si

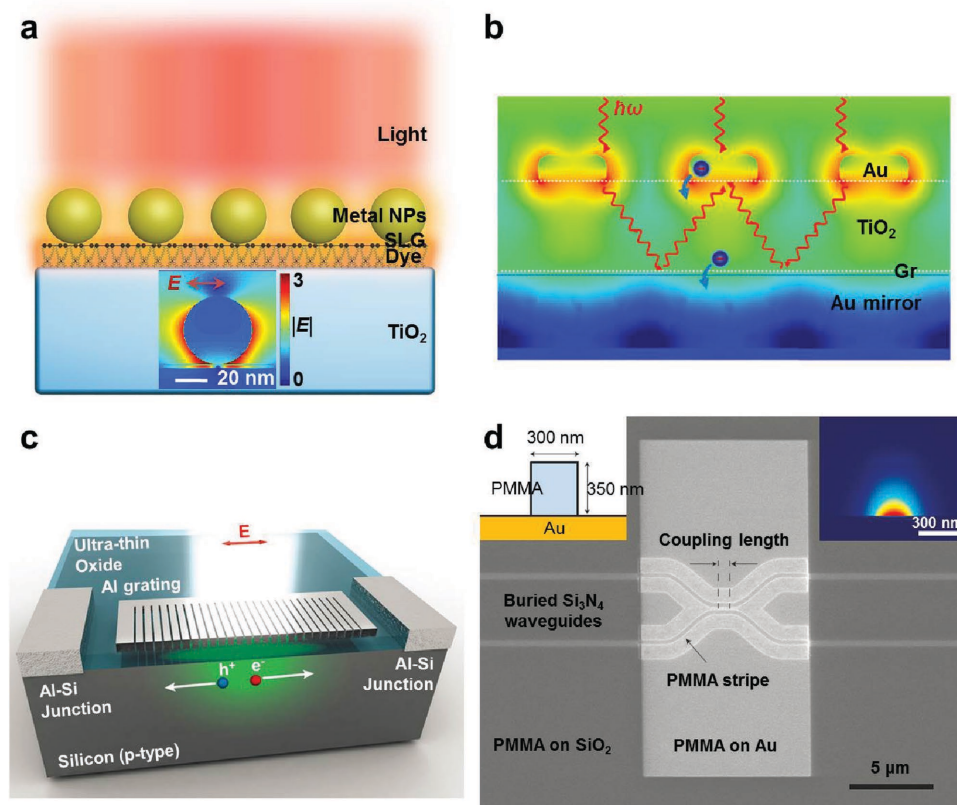


Figure 2. Applications of plasmon-induced light concentration. a) Substrate-induced interfacial plasmonics for photovoltaic conversion with a TiO₂/dye/graphene/plasmonic metal interface. The inset shows the side view of the electrical field distribution surrounding individual NPs in the TiO₂/dye/graphene/plasmonic metal system. b) Plasmon enhanced internal photoemission in an antenna-spacer-mirror based Au/TiO₂ nanostructure. c) Color-selective and CMOS-compatible photodetection based on Al plasmons. The insets show the schematic diagram (left) and energy distribution (right) for designed plasmonic waveguides. a) Reproduced with permission.^[11] Copyright 2015, Nature Publishing Group; b) Reproduced with permission.^[21] Copyright 2015, American Chemical Society; c) Reproduced with permission.^[22] Copyright 2014, John Wiley & Sons, Inc.; d) Reproduced with permission.^[25] Copyright 2014, Nature Publishing Group.

structure for realizing color selective detection (Figure 2c). For plasmon-enhanced photoluminescence, through fixing a plasmonic Ag nanodisc array to a large-area MoS₂ monolayer on SiO₂/Si substrates, Butun et al.^[23] demonstrated a 12-time enhanced photoluminescence of the MoS₂ monolayer due to the plasmon-induced interfacial light concentration.^[24] In addition to above-mentioned applications, with patterned dielectric polymethyl methacrylate (PMMA) loaded on Au films for surface plasmon polariton waveguides, Fakonas et al.^[25] have realized two-photon quantum interference between plasmons (Figure 2d), which helps to employ plasmonic devices in future quantum information applications.

3. Plasmon-Induced Hot Carriers

In addition to the remarkable capabilities of light trapping and electromagnetic field concentration, plasmonic nanostructures can also directly turn the collected optical energy into the electrical energy by generating hot carriers. Specifically, after light absorption, the plasmon excitation can nonradiatively decay into hot carrier states on a timescale ranging from 1 to 100 fs (Figure 3a). These plasmon-induced hot carriers in metals could be separated at the metal/semiconductor interface for further applications. Therefore, effective control of the metal/semiconductor interface for high-efficiency hot-carrier generation, separation and transport is of crucial importance to utilize these hot carriers in plasmonic heterostructures.

3.1. Plasmon-Induced Hot Carrier Generation

The decay of plasmon excitation to hot carriers is a pure quantum mechanical process, Landau damping, in which a plasmon quantum is transferred into an intraband excitation within the conduction band of the metal or an interband excitation between occupied bands (usually *d* bands) and the conduction band (Figure 3a). These different types of hot-carrier excitation are affected by the intrinsic material and architectural properties of plasmonic nanostructures, which determines the applications of plasmon-induced hot carriers. Through first principles calculations, Sundararaman et al.^[26] have systematically investigated plasmon-induced hot-carrier generation in typical plasmonic metal materials: Al, Au, Ag and Cu. Their calculations illustrated that interband transitions at higher plasmon energies dominate the initial energy distribution in plasmonic nanostructures, particularly for the structures with a large scale. The electronic band structures, especially the energy difference between the *d* bands and the Fermi level of the metals, could significantly affect the interband excited hot carriers. In detail, the generated hot holes in Cu and Au are more energetic than the generated hot electrons by 1–2 eV; the hot holes and electrons are with equitable narrow energy distributions in Ag and continuous energy distributions in Al. When the confining geometries of plasmonic structures become smaller, usually <20 nm, nano-confinement effects allow the intraband transitions to take place and alter the hot carrier distributions, which finitely generate hot

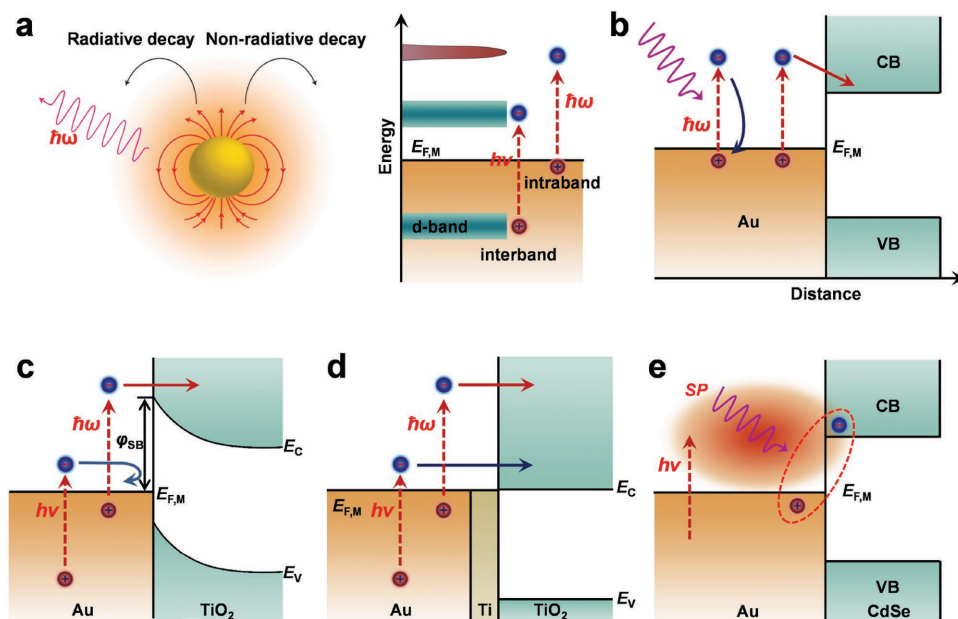


Figure 3. Plasmon-induced hot carriers. a) Plasmons in metal nanostructures can decay via a radiative path with re-emitting photons or via a nonradiative path with generating hot carriers. The nonradiative decay can proceed through intraband excitations or interband excitations. b) Hot electron transport near the interface, where hot electrons far away from the interface will recombine with hot holes. c) Band diagram schematic of a Au–TiO₂ Schottky device. The Schottky barrier prevents the carriers with low energy to cross over. d) Band diagram schematic of a Au–Ti–TiO₂ Ohmic device. A non effective Ohmic barrier allows for the collection of carriers with low energy. e) Plasmon-induced metal-to-semiconductor interfacial charge-transfer transition (PICTT) pathway, where the plasmon decays via directly creating an electron in the conduction band (CB) of CdSe and a hole in Au. a) Reproduced with permission.^[26] Copyright 2014, Nature Publishing Group; b) Reproduced with permission.^[26] Copyright 2014, Nature Publishing Group; c) Reproduced with permission.^[28] Copyright 2015, Nature Publishing Group; d) Reproduced with permission.^[28] Copyright 2015, Nature Publishing Group; e) Reproduced with permission.^[32] Copyright 2015, American Association for the Advancement of Science.

carriers at lower plasmon energies by directly exciting electrons from the Fermi level of plasmonic structures. Furthermore, the geometry of plasmonic structures can affect intrinsic plasmon resonance and thus the energy distribution of plasmon-induced intraband transitions.^[27] For instance, spherical Au nanoparticles support a single plasmon resonance in the visible range, while Au nanorods exhibit both longitudinal and transverse plasmon resonances, where the longitudinal resonance could be tuned to the near-infrared region with lower energy by increasing the nanorod aspect ratio. Hence, the initial hot carrier distributions in plasmonic structures can be effectively controlled by optimized material selection and geometry design.

3.2. Plasmon-Induced Hot Carrier Transport

To efficiently utilize plasmon-induced hot carriers, they should be transported to the metal/semiconductor interface for collection. However, the generated hot carriers far from the interface can lose energy through scattering, recombination or other processes, and finally be prevented to cross over the Schottky barrier for further applications (Figure 3b). Only the generated hot carriers close to the interface within the mean-free path (25 nm for Au) can be transported to the interface for collection.^[28] Therefore, for effectively utilizing plasmonic hot carriers, the density of generated hot carriers should be increased near the interface within the mean-free path. Through ultrafast temporal and spectral detections of excited plasmonic hot electrons in metal/semiconductor nanostructures, Harutyunyan et al.^[29] found that most plasmonic hot electrons were generated from hot spots of the system, where the concentrated electromagnetic field was strong due to plasmon resonant coupling. Therefore, concentrating the plasmon-induced electromagnetic field to the metal/semiconductor interface, such as substrate-induced interfacial plasmon or plasmonic coupling between metal nanostructures,^[20,21] helps to enhance both the hot carrier generation in plasmonic metals and further transport to the interface for collection.

3.3. Plasmon-Induced Hot Carrier Collection

For plasmonic hot carrier collection, hot carriers usually need to cross over a Schottky barrier at the metal/semiconductor interface, where the effective physical contact between the metal and the semiconductor is a key factor.^[30] In detail, when hot electrons have energies higher than the Schottky barrier energy, they can be injected into the semiconductor with matched conduction bands. In addition, hot electrons with a lower energy could also tunnel across the barrier to the semiconductor, but with a much lower possibility. Therefore, to effectively utilize plasmon-induced hot carriers with specific distributions, metal/semiconductor interface engineering with the matched Schottky barrier are necessary for efficiently collecting hot carriers. As the Schottky barrier height for electrons at the metal/semiconductor interface is determined

by the energy level difference between the Fermi level of the metal and the conduction band of the semiconductor, in most cases choosing the appropriate metallic nanostructure and semiconductor materials with the matched energy levels is an effective way for tuning the Schottky barrier.^[28] For a specific metal/semiconductor interface, interface modification can also be used for adjusting the barrier. Through adjusting the contact barrier, Zheng et al.^[28] found that the Schottky contact at the Au/TiO₂ interface could only allow the interband excited plasmonic hot electrons, which have higher energy than the intraband excited plasmonic hot electrons from the *d* band, to cross over (Figure 3c). When a layer of Ti with a thickness of 2 nm was incorporated into the Au/TiO₂ interface, the Ti layer aligned the Fermi level of Au with the conduction band of TiO₂ to form an Ohmic contact with no barrier for electrons. For such an Ohmic contact, low-energy hot electrons could also cross over the interface. As a result, both plasmonic intraband higher-energy hot electrons and interband lower-energy hot electrons can be collected (Figure 3d). In addition, when a 1–2 nm Ti adhesion layer was incorporated into the Au/Si interface, the height of the Au/Si Schottky barrier was reduced from ≈1.1 eV to ≈0.5 eV. This lower Au/Ti/Si Schottky barrier permitted plasmonic hot electrons with a lower energy, which were generated from the nanorods with longitudinal plasmon resonance excitation at the near-infrared region, to be collected.^[27]

In addition to the suitable barrier height at the interface, the efficiency for hot carrier collection is mainly determined by the competition between the effective hot carrier injection process and ineffective energy relaxation and electron-hole recombination processes. Therefore, fast injection of hot carriers is necessary for efficient carrier collection, which is controlled by the coupled density of states (DOS) between the metal and the semiconductor. For instance, in an Au/TiO₂ system,^[31] due to the high *d*-orbital DOS in the conduction band of TiO₂, hot electrons can inject into TiO₂ on a sub-100 fs time scale, which is faster than the intrinsic carrier relaxation process in Au nanostructures on a 100 fs to 1 ps timescale and electron-hole recombination at the trap sites of Au/TiO₂ interface on a 1 ps to nanoseconds timescale. When the interdomain coupling and mixing between metallic nanostructures and semiconductor levels become strong enough, a new plasmon decay pathway could be opened at the metal/semiconductor interface for separating plasmon-induced electron-hole pairs with high efficiency. In detail, as shown in Figure 3e, the decay of plasmons could directly excite an electron from the metal to a strongly coupled semiconductor, which directly creates an electron in the conduction band of the semiconductor and a hole in the metal. Such plasmon induced metal-to-semiconductor interfacial charge transfer transition (PICTT) pathway is more effective for plasmon induced electron-hole pair separation at the interface than the traditional plasmon induced hot-electron transfer (PHET) pathway. For instance, in an Au/CdSe system,^[32] the strong coupling between the electronic levels of Au and CdSe led to a strongly damped Au plasmon and highly efficient plasmon-induced electron-hole pair separation with a quantum efficiency >24% at the Au/CdSe interface by the PICTT pathway.

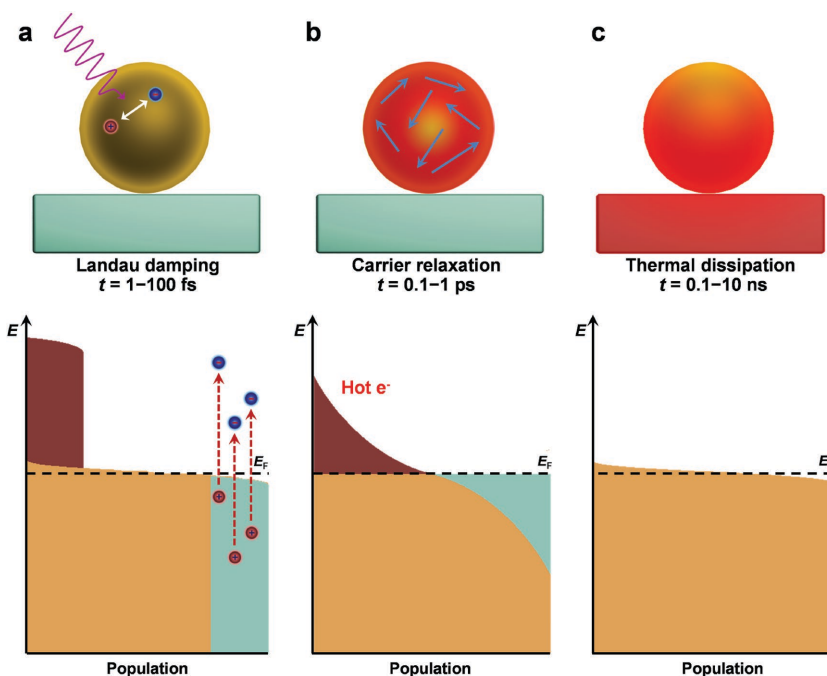


Figure 4. Plasmon-induced local heat in plasmonic nanostructures. a–c) Schematic representations of the Landau damping, carrier relaxation and thermal dissipation processes with the corresponding population of the electronic states. Hot electron distributions are represented by the crimson areas above the Fermi energy E_F and hot holes are represented by the cyan area below E_F . Reproduced with permission.^[2f] Copyright 2015, Nature Publishing Group.

3.4. Plasmon-Induced Hot Carrier Decay for Local Heating

When plasmon-induced hot carriers generated in metals cannot be effectively separated from each other for injection into adjacent semiconductors or molecules for further applications, the hot carriers will decay into local heat. Through electron–electron scattering processes, the hot carriers will realize their energy redistribution within a timescale ranging from 0.1 ps to 1 ps, which leads to remarkable heating of the plasmonic nanostructure itself (Figure 4a,b); next, on a longer timescale ranging from 0.1 ns to 10 ns, the local heat will be further transferred from the nanostructure itself to its surrounding environment by thermal conduction (Figure 4c).^[2f]

For plasmonic nanoparticles dispersed in liquids, plasmon-induced local heating under irradiation with the matched laser could boil the liquid and lead to the formation of nanobubbles surrounding the plasmonic particle. Through systematically studying the bubble formation process at an individual metallic nanoparticle, Fang et al.^[33] found that the rate of plasmon-induced heat generation is proportional to the optical absorption cross-section of plasmonic nanostructures multiplied by the incident optical intensity. With the increase of the laser power and the decrease of the nanoparticle size, the localized heating can be enhanced within a certain range. Furthermore, Hogan et al.^[34] found that the light trapping effect, which arises from the collective effect mediated by multiple light scattering from the plasmonic nanoparticles, could be coupled with the hot carrier decay for providing intense localized heating.

3.5. Applications of Plasmon-Induced Hot Carriers

Through interface engineering in metal/semiconductor heterostructures, the generation, transport and collection of plasmon-induced hot carriers can be effectively controlled at the interface, which ensures the efficient utilization of plasmon-induced hot carriers for photodetecting, photovoltaic and photocatalytic applications. For instance, in an interface engineered Au/Ti/Si photodetector (Figure 5a), hot carriers generated from plasmon excited gratings in the near-infrared region can be effectively collected at the Schottky interface for producing photocurrent, thus realizing narrowband photodetection in the near-infrared region.^[35] With plasmon-induced hot carrier generation in Au nanorods and collection at the Au/TiO₂ Schottky interface, Mubeen et al.^[36] demonstrated the fabrication of a wholly plasmonic photovoltaic device (Figure 5b). In addition, because plasmon-induced hot carriers exhibit both reduction and oxidation activities, they are widely utilized in many photocatalytic systems. For example, through collecting hot electrons by the capped TiO₂ layer, which was further decorated with platinum nanoparticles as the hydrogen

evolution catalyst, and hot holes by the cobalt-based oxygen evolution catalyst (Co-OEC) on Au nanorods, Mubeen et al.^[37] have achieved an autonomous plasmonic solar water splitter (Figure 5c). By using the presynthesized colloidal Au nanoparticles and a designed ligand-exchange method, Ding et al.^[38] synthesized uniform plasmonic Au/TiO₂ photocatalysts with close Au/TiO₂ Schottky contacts, which displayed the superior plasmonic photocatalytic activity for dye decomposition under visible-light illumination. Furthermore, as the plasmon-induced electron-hole energy distributions can be effectively controlled in plasmonic nanostructures, plasmon-induced hot carriers could be used for photocatalyzing mild organic oxidation-reduction reactions in a controllable manner. For example, with Au nanoparticles (NPs) with a bimodal size on TiO₂ for controlling both size dependent energy distributions and charge transport of plasmon-induced hot carriers, both plasmon-induced photocatalytic reduction from nitrobenzenes to azobenzenes and photocatalytic oxidation from isopropanol to acetone could occur in plasmonic nanostructures (Figure 5d).^[39] In addition to the injection of hot carriers to semiconductors, the hot carriers can be also directly injected into absorbed molecules for hot-carrier assisted photocatalysis. For example, Christopher et al.^[40] found that hot electrons in plasmonic Ag nanostructures could be injected into absorbed O₂ on the surface for forming an active transient negative-ion state, which can be used for different kinds of catalytic oxidation reactions, such as ethylene epoxidation, CO oxidation and NH₃ oxidation.

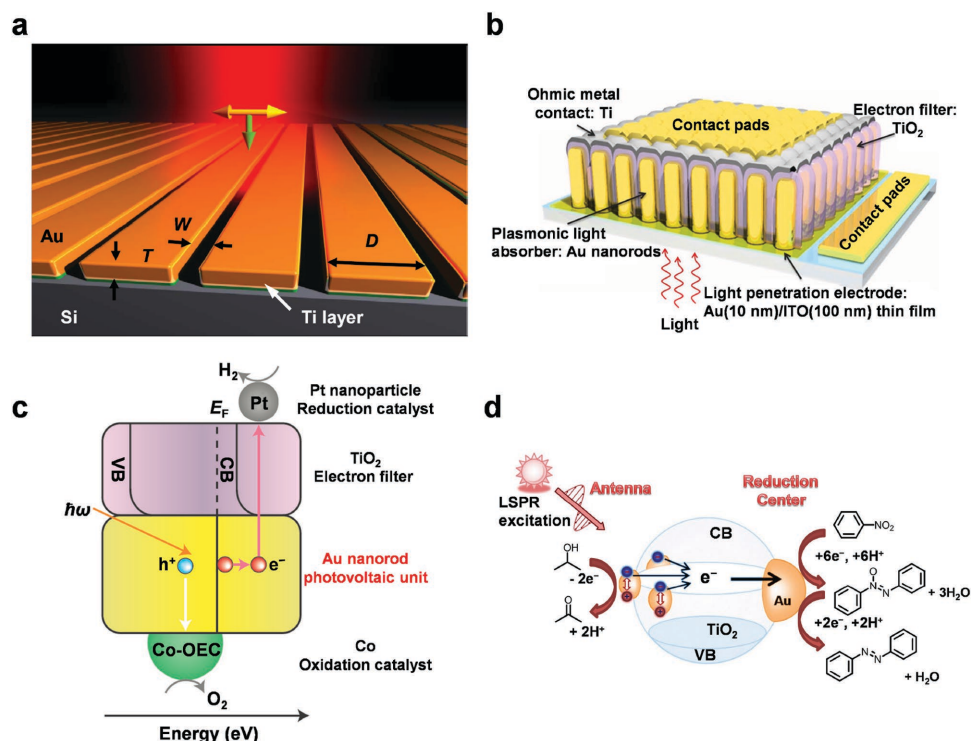


Figure 5. Applications of plasmon-induced hot carriers. a) Narrowband photodetection in the near-infrared region with a plasmon-induced hot electron device. b) Plasmonic photovoltaics. c) An autonomous photosynthetic device in which all charge carriers derive from surface plasmons. d) Plasmon-induced photocatalytic reduction and oxidation. a) Reproduced with permission.^[35] Copyright 2013, Nature Publishing Group; b) Reproduced with permission.^[36] Copyright 2014, American Chemical Society; c) Reproduced with permission.^[37] Copyright 2013, Nature Publishing Group; d) Reproduced with permission.^[39] Copyright 2014, John Wiley & Sons, Inc.

4. Plasmon-Induced Energy Transfer

In addition to plasmon-induced light trapping and hot-carrier injection effects, another important factor of influencing the final efficiency in different applications of plasmonic metal/semiconductor nanocomposites is plasmonics-modulated energy transfer at the heterointerfaces. In the following section, we systematically illustrate such plasmon-induced energy transfer at the metal/semiconductor interface and its applications.

4.1. Plasmon-Induced Resonance Energy Transfer

Due to the dipole-dipole coupling between the plasmon excited metal and the adjacent semiconductor with partially overlapped spectra, as shown in **Figure 6**, not only the absorbed energy in a plasmonic metal can transfer forward to a semiconductor, which leads to the plasmonic enhancement of semiconductor excitation, but also the excited energy in a semiconductor can transfer backward to a metal, which leads to the quenching of the excited semiconductor.^[41] For the forward energy transfer, if spectral overlap exists between the plasmon excitation of the metal and the band absorption of the semiconductor and the semiconductor is spatially located within the plasmon's near field,^[30] via dipole-dipole coupling the plasmonic energy can coherently transfer from a metal to a semiconductor before the

dephasing of the collective dipole moment of plasmonic metals, which is also called a plasmon-induced resonance energy transfer (PIRET) process. For the backward energy transfer, the thermal relaxation of the excited carriers in semiconductors usually occurs before the energy is transferred from a semiconductor to a metal by an incoherent Förster resonance energy transfer (FRET) process, which has a Stoke's shift to the red-shifted direction in most cases.

It is well known that energy transfer induced by dipole-dipole coupling between donors and acceptors is proportional to their dipole moments, and the materials with larger dipole moments tend to provide energy. In addition, the dephasing times of the dipoles also have crucial effects on the direction of energy transfer. In general, the dipole with the short dephasing time builds up an incoherent state more quickly and thus traps more energy. In traditional plasmonic metal/semiconductor systems, the dipole moment resulted from plasmons in metals with the collective motion of many conduction electrons is an order of magnitude larger than that of the interband transition of semiconductors. The dephasing times for both dipoles are similar in most cases, wherein the relative plasmon-to-semiconductor dephasing times can be partially changed by interface dampening at the metal/semiconductor contact interface. Therefore, the energy is usually efficiently transferred from plasmon-excited metals to semiconductors, which can be used for generating electron-hole excitation below and near the semiconductor band edge

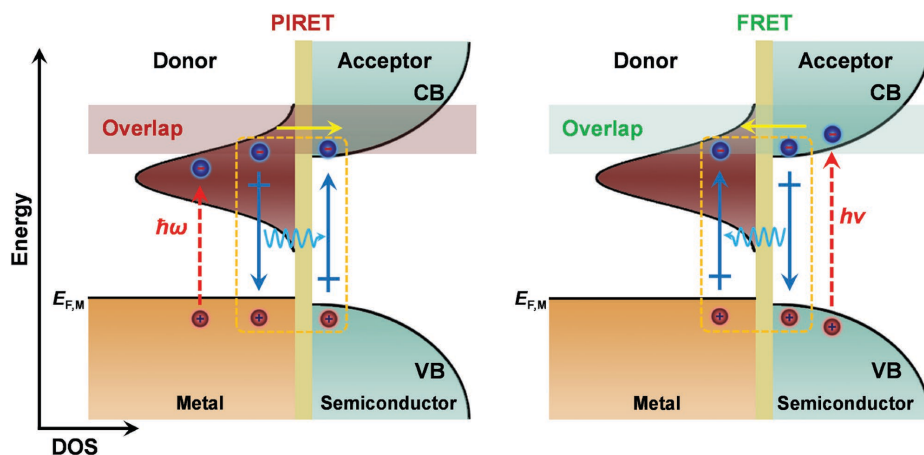


Figure 6. Resonance energy transfer at the plasmonic metal/semiconductor interface. For plasmon-induced resonance energy transfer, the plasmon is excited and its energy is transferred to the semiconductor (left). For Förster resonance energy transfer (FRET), the semiconductor is excited and its energy is transferred to the plasmon (right). Reproduced with permission.^[41] Copyright 2015, Nature Publishing Group.

(Figure 7a).^[42] In the case of the sole excitation of semiconductors, energy can also transfer from a semiconductor to a metal, which leads to the partial quenching of semiconductors at that excitation wavelength. In general, the efficiency of energy transfer induced by dipole-dipole coupling is greatly

affected by the distances between the two dipoles. At a long distance, the electric field decays as $1/d^6$, where d denotes the distance between the centers of the two nanoparticles. However, at a shorter distance, the electric field decays as $1/s^4$ (s is the distance between the surface of the nanoparticles),

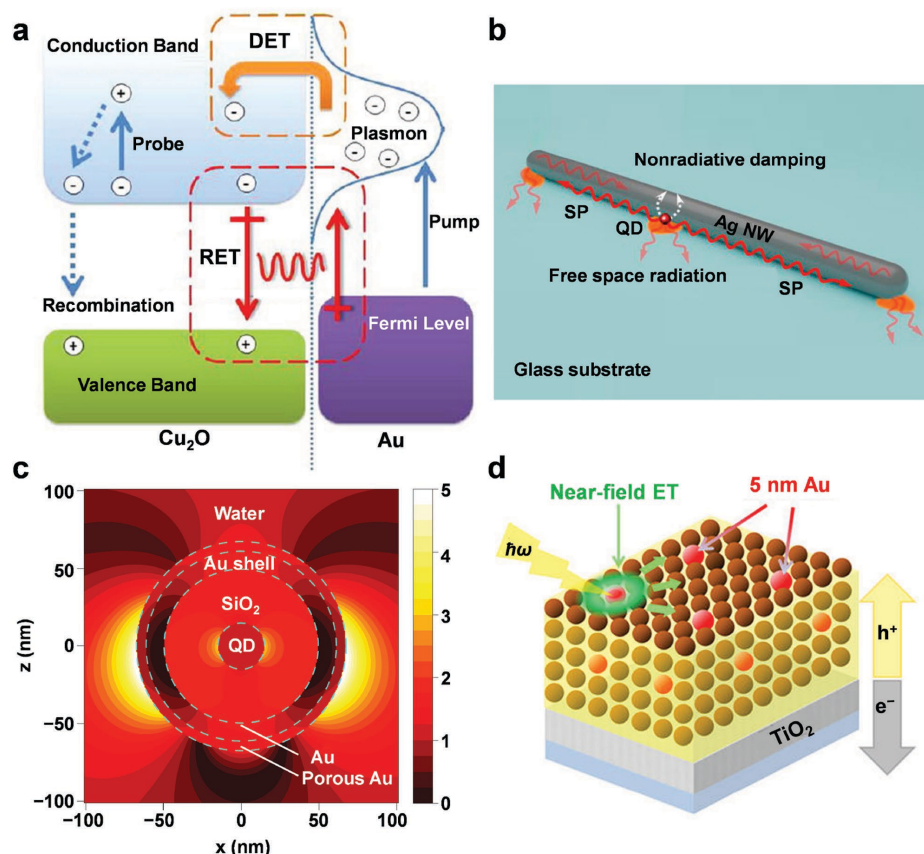


Figure 7. Applications of plasmon-induced resonance energy transfer. a) Photocatalytic activity enhanced by plasmonic resonant energy transfer from a metal to a semiconductor. b) Quantum emitters comprising a quantum dot coupled with an Ag nanowire. c) Non-blinking quantum dot with a plasmonic nanoshell resonator. d) Plasmonic nanocrystal solar cell utilizing strongly confined radiation. a) Reproduced with permission.^[42] Copyright 2012, American Chemical Society; b) Reproduced with permission.^[44] Copyright 2015, American Chemical Society; c) Reproduced with permission.^[45] Copyright 2015, Nature Publishing Group; d) Reproduced with permission.^[46] Copyright 2014, American Chemical Society.

because the curved surface of the plasmonic nanoparticle can be approximated as a flat surface.

4.2. Applications of Plasmon-Induced Resonance Energy Transfer

By selecting matched plasmonic metal and semiconductor materials, and modifying the metal/semiconductor contact interface, the plasmon-induced resonance energy transfer pathways can be effectively controlled and then the transferred plasmonic energy can be utilized for many plasmonic enhanced applications.^[43] For instance, in a plasmonic enhanced photoluminescence system composed of a Ag nanowire and a single quantum dot emitter (Figure 7b), through controlling the plasmon-induced resonance energy transfer path by tuning the emitter-nanowire distance with a Al₂O₃ interlayer, plasmonic enhanced photoluminescence of the emitter reached an optimized efficiency at the distance of 10 nm.^[44] In another photoluminescence emitter hybridized with a single CdSe/CdS quantum dot core which was encapsulated in a SiO₂ shell and further coated with a layer of Au nanoshell (Figure 7c), the plasmon-induced resonance energy transfer from the plasmonic Au nanoshell resonator to the quantum dot core provided the emitter with a non-blinking and Poissonian emission.^[45] In mixed (Au, PbS) solar cells (Figure 7d), the interface passivation by 5 nm Au nanoparticles, which have strong confined radiation, with a thin layer of wide gap semiconductor, could support effectively plasmon-induced resonant energy transfer from Au nanoparticles to PbS nanocrystals, thus enhancing power conversion efficiency.^[46] For photocatalytic O₂ evolution reaction at composite photoelectrodes with Ag nanocubes on nitrogen-doped TiO₂ (N-TiO₂) films, the plasmon-induced resonance energy transfer from plasmonic Ag nanocubes to neighboring N-TiO₂ semiconductors generated electron-hole pairs near the N-TiO₂ semiconductor surface, which were further effectively separated from each other and then easily transported to the surface to be used for photocatalytic reactions.^[47] It is worthwhile to mention that PIRET is most efficient to enhance the efficiency of plasmon-based solar energy conversion in photovoltaics (PV) and photo-electrochemical cells (PEC).^[48] When the plasmon energy overlaps the semiconductor's band edge, the large dipole moment of the plasmon allows strong light absorption and further effective energy transfer to the semiconductor, thus extending the semiconductor's photoconversion range. In particular, for a plasmon energy of ≈ 1.9 eV and a semiconductor bandgap of ≈ 1.8 eV, ≈ 2.3 enhancement of PV efficiency can be achieved, where PIRET dominates the largest enhancement. Therefore, plasmonics can be utilized to restore solar energy conversion of a weakly absorbing semiconductor to its Shockley-Queisser (SQ) limit.

5. Conclusions and Perspectives

The plasmon-induced interfacial processes in plasmonic metal/semiconductor heterostructures can be summarized as follows. With the screening effect of dielectric semiconductors, the additional plasmonic nanocavity and further coupling

with hot spots, light energy could be trapped at the metal/semiconductor interface through photoexcitation of plasmonic metals to form the local electromagnetic field. Such plasmon resonance-mediated local electromagnetic field can be used to excite the intrinsic interband transitions of adjacent semiconductors through either light scattering mechanism or plasmonic radiative mechanism, wherein the light energy needs to be larger than the band gap of the excited semiconductors. On the other hand, after plasmonic excitation of metal nanostructures, plasmon excitation can decay into hot electron-hole pairs by a nonradiative decoherent process. These hot carriers can further inject into the adjacent semiconductor by the direct charge transport process, which requires the matched electronic energy levels at the interface. In addition, when the plasmon-excited metal and adjacent semiconductor have a large spectral overlap, the plasmonic energy in metals can be resonantly transferred to semiconductors and excite them before the dephasing of the collective dipole moment. Therefore, these plasmon-induced light trapping, hot carrier generation/transport, and energy transfer processes at the heterointerfaces can be efficiently regulated. To fully utilize these unique plasmonic properties of metal/semiconductor nanostructures that would combine electronic and photonic components in the same device for a wide variety of applications, selection of matched materials and design of optimized interfaces are in urgent need to control these interfacial effects for realizing the high-performance devices, which invites future intense research activities.

Acknowledgements

C.J. and X.L. contributed equally to this work. The authors acknowledge Prof. Zheyu Fang from School of Physics in Peking University for helpful discussions. This work was primarily supported by NSFC (21225311, 91333102, 21373014 and 11222431) and 973 Project (2012CB921404 and 2012CB921403).

Received: February 26, 2016

Revised: May 1, 2016

Published online:

- [1] a) O. Ekmel, *Science* **2006**, *311*, 189; b) J. A. Schuller, E. S. Barnard, W. S. Cai, Y. C. Jun, J. S. White, M. L. Brongersma, *Nat. Mater.* **2010**, *9*, 193; c) P. Albert, *Science* **2008**, *322*, 868.
- [2] a) R. Jiang, B. Li, C. Fang, J. Wang, *Adv. Mater.* **2014**, *26*, 5274; b) S. Lincic, P. Christopher, D. B. Ingram, *Nat. Mater.* **2011**, *10*, 911; c) S. T. Kochuveedu, Y. H. Jang, D. H. Kim, *Chem. Soc. Rev.* **2013**, *42*, 8467; d) P. Zhang, T. Wang, J. Gong, *Adv. Mater.* **2015**, *27*, 5328; e) C. Wang, D. Astruc, *Chem. Soc. Rev.* **2014**, *43*, 7188; f) M. L. Brongersma, N. J. Halas, P. Nordlander, *Nat. Nanotechnol.* **2015**, *10*, 25; g) C. Clavero, *Nat. Photonics* **2014**, *8*, 95; h) S. K. Cushing, N. Wu, *J. Phys. Chem. Lett.* **2016**, *7*, 666.
- [3] N. S. King, M. W. Knight, N. Large, A. M. Goodman, P. Nordlander, N. J. Halas, *Nano Lett.* **2013**, *13*, 5997.
- [4] M. W. Knight, Y. Wu, J. B. Lassiter, P. Nordlander, N. J. Halas, *Nano Lett.* **2009**, *9*, 2188.
- [5] Z. Xu, Y. Lin, M. Yin, H. Zhang, C. Cheng, L. Lu, X. Xue, H. J. Fan, X. Chen, D. Li, *Adv. Mater. Interfaces* **2015**, *2*, 1500169.
- [6] S. Zhang, K. Bao, N. J. Halas, H. Xu, P. Nordlander, *Nano Lett.* **2011**, *11*, 1657.

- [7] G. Li, C. Cherqui, N. W. Bigelow, G. Duscher, P. J. Straney, J. E. Millstone, D. J. Masiello, J. P. Camden, *Nano Lett.* **2015**, *15*, 3465.
- [8] Y. J. Lu, J. Kim, H. Y. Chen, C. Wu, N. Dabidian, C. E. Sanders, C. Y. Wang, M. Y. Lu, B. H. Li, X. Qiu, *Science* **2012**, *337*, 1.
- [9] S. Mokkaapati, D. Saxena, N. Jiang, L. Li, H. H. Tan, C. Jagadish, *Nano Lett.* **2015**, *15*, 307.
- [10] Z. Li, Y. Xiao, Y. Gong, Z. Wang, Y. Kang, S. Zu, P. M. Ajayan, P. Nordlander, Z. Fang, *ACS Nano* **2015**, *9*, 10158.
- [11] X. Li, C. Jia, B. Ma, W. Wang, Z. Fang, G. Zhang, X. Guo, *Sci. Rep.* **2015**, *5*, 14497.
- [12] L. V. Brown, X. Yang, K. Zhao, B. Y. Zheng, P. Nordlander, N. J. Halas, *Nano Lett.* **2015**, *15*, 1272.
- [13] A. Sobhani, A. Manjavacas, Y. Cao, M. J. McClain, F. J. Garcia de Abajo, P. Nordlander, N. J. Halas, *Nano Lett.* **2015**, *15*, 6946.
- [14] A. Casadei, E. F. Pecora, J. Trevino, C. Forestiere, D. Ruffer, E. Russo-Averchi, F. Matteini, G. Tutuncuoglu, M. Heiss, A. Fontcuberta i Morral, L. Dal Negro, *Nano Lett.* **2014**, *14*, 2271.
- [15] a) Z. Fang, Y. Wang, L. Zheng, A. Schlather, P. M. Ajayan, F. H. L. Koppens, P. Nordlander, N. J. Halas, *ACS Nano* **2012**, *6*, 10222; b) Z. Fang, Z. Liu, Y. Wang, P. M. Ajayan, P. Nordlander, N. J. Halas, *Nano Lett.* **2012**, *12*, 3808.
- [16] S. Brittman, H. Gao, E. C. Garnett, P. Yang, *Nano Lett.* **2011**, *11*, 5189.
- [17] I. Thomann, B. A. Pinaud, Z. Chen, B. M. Clemens, T. F. Jaramillo, M. L. Brongersma, *Nano Lett.* **2011**, *11*, 3440.
- [18] J. Li, S. K. Cushing, P. Zheng, F. Meng, D. Chu, N. Wu, *Nat. Commun.* **2013**, *4*, 2651.
- [19] S. Ramadurgam, T. G. Lin, C. Yang, *Nano Lett.* **2014**, *14*, 4517.
- [20] Y. C. Pu, G. Wang, K. D. Chang, Y. Ling, Y. K. Lin, B. C. Fitzmorris, C. M. Liu, X. Lu, Y. Tong, J. Z. Zhang, Y. J. Hsu, Y. Li, *Nano Lett.* **2013**, *13*, 3817.
- [21] Y. Fang, Y. Jiao, K. Xiong, R. Ogier, Z. J. Yang, S. Gao, A. B. Dahlin, M. Kall, *Nano Lett.* **2015**, *15*, 4059.
- [22] B. Y. Zheng, Y. Wang, P. Nordlander, N. J. Halas, *Adv. Mater.* **2014**, *26*, 6318.
- [23] S. Butun, S. Tongay, K. Aydin, *Nano Lett.* **2015**, *15*, 2700.
- [24] Y. Kang, S. Najmaei, Z. Liu, Y. Bao, Y. Wang, X. Zhu, N. J. Halas, P. Nordlander, P. M. Ajayan, J. Lou, Z. Fang, *Adv. Mater.* **2014**, *26*, 6467.
- [25] J. S. Fakanas, H. Lee, Y. A. Kelaita, H. A. Atwater, *Nat. Photonics* **2014**, *8*, 317.
- [26] R. Sundararaman, P. Narang, A. S. Jermyn, W. A. Goddard III, H. A. Atwater, *Nat. Commun.* **2014**, *5*, 5788.
- [27] M. W. Knight, H. Sobhani, P. Nordlander, N. J. Halas, *Science* **2011**, *332*, 702.
- [28] B. Y. Zheng, H. Zhao, A. Manjavacas, M. McClain, P. Nordlander, N. J. Halas, *Nat. Commun.* **2015**, *6*, 7797.
- [29] H. Harutyunyan, A. B. F. Martinson, D. Rosenmann, L. K. Khorashad, L. V. Besteiro, A. O. Govorov, G. P. Wiederrecht, *Nat. Nanotechnol.* **2015**, *10*, 770.
- [30] S. K. Cushing, J. Li, J. Bright, B. T. Yost, P. Zheng, A. D. Bristow, N. Wu, *J. Phys. Chem. C* **2015**, *119*, 16239.
- [31] R. Long, O. V. Prezhdo, *J. Am. Chem. Soc.* **2014**, *136*, 4343.
- [32] K. Wu, J. Chen, J. R. McBride, T. Lian, *Science* **2015**, *349*, 632.
- [33] Z. Fang, Y. R. Zhen, O. Neumann, A. Polman, F. J. Garcia de Abajo, P. Nordlander, N. J. Halas, *Nano Lett.* **2013**, *13*, 1736.
- [34] N. J. Hogan, A. S. Urban, C. Ayala-Orozco, A. Pimpinelli, P. Nordlander, N. J. Halas, *Nano Lett.* **2014**, *14*, 4640.
- [35] A. Sobhani, M. W. Knight, Y. Wang, B. Zheng, N. S. King, L. V. Brown, Z. Fang, P. Nordlander, N. J. Halas, *Nat. Commun.* **2013**, *4*, 1643.
- [36] S. Mubeen, J. Lee, W. R. Lee, N. Singh, G. D. Stucky, M. Moskovits, *ACS Nano* **2014**, *8*, 6066.
- [37] S. Mubeen, J. Lee, N. Singh, S. Kramer, G. D. Stucky, M. Moskovits, *Nat. Nanotechnol.* **2013**, *8*, 247.
- [38] D. Ding, K. Liu, S. He, C. Gao, Y. Yin, *Nano Lett.* **2014**, *14*, 6731.
- [39] S. Naya, T. Niwa, T. Kume, H. Tada, *Angew. Chem. Int. Ed.* **2014**, *53*, 7305.
- [40] P. Christopher, H. Xin, S. Linic, *Nat. Chem.* **2011**, *3*, 467.
- [41] J. Li, S. K. Cushing, F. Meng, T. R. Senty, A. D. Bristow, N. Wu, *Nat. Photonics* **2015**, *9*, 601.
- [42] S. K. Cushing, J. Li, F. Meng, T. R. Senty, S. Suri, M. Zhi, M. Li, A. D. Bristow, N. Wu, *J. Am. Chem. Soc.* **2012**, *134*, 15033.
- [43] Z. Li, R. Ye, R. Feng, Y. Kang, X. Zhu, J. M. Tour, Z. Fang, *Adv. Mater.* **2015**, *27*, 5235.
- [44] Q. Li, H. Wei, H. Xu, *Nano Lett.* **2015**, *15*, 8181.
- [45] B. Ji, E. Giovanelli, B. Habert, P. Spinicelli, M. Nasilowski, X. Xu, N. Lequeux, J. P. Hugonin, F. Marquier, J. J. Greffet, B. Dubertret, *Nat. Nanotechnol.* **2015**, *10*, 170.
- [46] K. Natalia, M. Pavel, R. Upendra, B. Ebin, U. Prakash, L. Geethika, R. Anton, A. D. Ostrowski, Z. Mikhail, *ACS Nano* **2014**, *8*, 12549.
- [47] D. B. Ingram, S. Linic, *J. Am. Chem. Soc.* **2011**, *133*, 5202.
- [48] S. K. Cushing, A. D. Bristow, N. Wu, *Phys. Chem. Chem. Phys.* **2015**, *17*, 30013.